THE JOURNAL OF PHYSICAL CHEMISTRY A

Article

Photoelectron Spectroscopy of the Hexafluorobenzene Cluster Anions: $(C_6F_6)_n^-$ (n = 1 – 5) and $I^-(C_6F_6)$

Joshua P. Rogers, Cate Sara Anstöter, James N Bull, Basile F. E. Curchod, and Jan R. R. Verlet

J. Phys. Chem. A, **Just Accepted Manuscript** • DOI: 10.1021/acs.jpca.8b11627 • Publication Date (Web): 29 Jan 2019

Photoelectron Spectroscopy of the Hexafluorobenzene Cluster Anions: $(C_6F_6)_n^-$ (n = 1 – 5) and $I^-(C_6F_6)$

*Joshua P. Rogers, Cate S. Anstöter, James N. Bull, Basile F. E. Curchod and Jan R. R. Verlet**

Department of Chemistry, Durham University, Durham DH1 3LE

ABSTRACT

Frequency-resolved (2D) photoelectron (PE) spectra of the anionic clusters $(C_6F_6)_n^-$, for n = 1 – 5, and time-resolved PE spectra of $I^-C_6F_6$ are presented using a newly built instrument and supported by electronic structure calculations. From the 2D PE spectra, the vertical detachment energy (VDE) of $C_6F_6^-$ was measured to be 1.60 ± 0.01 eV and the adiabatic detachment energy (ADE) ≤ 0.70 eV. The PE spectra also contain fingerprints of resonance dynamics over certain photon energy ranges, in agreement with the calculations. An action spectrum over the lowest resonance is also presented. The 2D spectra of $(C_6F_6)_n^-$ show that the cluster can be described as $C_6F_6^-(C_6F_6)_{n-1}$. The VDE increases linearly (200 ± 20 meV n^{-1}) due to the stabilising influence on the anion of the solvating C_6F_6 molecules. For $I^-C_6F_6$, action spectra of the absorption just below both detachment channels are presented. Time-resolved PE spectra of $I^-C_6F_6$ excited at 3.10 eV and probed at 1.55 eV reveal a short-lived non-valence state of $C_6F_6^-$ that coherently evolves into the valence ground state of the anion and induces vibrational motion along a specific buckling coordinate. Electronic structure calculations along the displacement of this mode show that at the extreme buckling angle, the probe can access an excited state of the anion that is bound at that geometry, but adiabatically unbound. Hence, slow electrons are emitted and show dynamics that probe predominantly the outer-turning point of the motion. A PE spectrum taken at t = 0 contains vibrational structure, assigned to a specific Raman and/or IR active mode of C_6F_6.

e-mail: j.r.r.verlet@durham.ac.uk

INTRODUCTION

Hexafluorobenzene, C_6F_6, has been extensively studied in electron attachment experiments as a text-book case in which the additional electron captured in the valence orbital of the anion leads to a dramatic Jahn-Teller distortion of the planar D_{6h} geometry associated with the neutral[1-7]. More recently, it has been theoretically suggested that the C_6F_6 anion, $C_6F_6^-$, also possesses a non-valence state for which the electron binding is predominantly driven by correlation forces[8]. This diffuse orbital associated with the neutral geometry of C_6F_6 provides a door-way state to the formation of valence-bound $C_6F_6^-$ and the dynamics of this attachment process have recently been probed in real-time[9]. Beyond the interaction of a single electron with a single C_6F_6 molecule, C_6F_6 also has some remarkable bulk properties. The electron mobility in liquid C_6F_6 is an order of magnitude larger than that expected from the motion of molecular anions through the liquid,[2] suggesting that the excess electron passes from one molecule to its neighbour without causing a change in the geometry of either molecule from a neutral planar configuration. Additionally, C_6F_6 is an exceedingly efficient scavenger of excess electrons in the non-attaching molecular liquid tetramethylsilane[2], again suggesting an efficient electron accepting pathway. In a recent study, we have shown evidence for non-valence states in anionic clusters of C_6F_6, where a low energy outgoing electron produced by photodetachment from $(C_6F_6)_n^-$ (where $n = 2 – 5$) was observed to be recaptured, leading to an indirect electron loss channel[10]. Finally, two-photon photoemission and scanning tunnelling microscopy experiments of C_6F_6 on Cu(111) surfaces point to the formation of diffuse anion states during the electron-capture process[3,11].

Given the interest in electron attachment to C_6F_6, there have been a number of studies[3,12-14] on $C_6F_6^-$, including two PE spectroscopy studies[15,16]. Kaya and coworkers measured the PE spectra of $(C_6F_6)_n^-$ with $n = 1 – 8$ at a photon energy, $h\nu = 3.49$ eV, as well as that of $AuC_6F_6^-$. Later, Bowen and coworkers studied $C_6F_6^-(H_2O)_n$ with $n = 0 – 2$ at $h\nu =$

2.54 eV. Both studies found the PE spectra of $C_6F_6^-$ to be very broad and with a vertical detachment energy of 1.55 eV. While the two experiments had overall agreement, the PE spectra of Bowen and coworkers showed additional vibrational structure on the broad PE profile. In the present study, we extend these previous works and probe the PE at a range of different *hv* as well as probing to higher *hv*, where new detachment channels become accsessible.

Performing PE spectroscopy over a range of *hv* can provide complementary information regarding the electron attachment process by virtue of its half-reaction equivalent[17-19]. Specifically, it is complementary to 2D electron energy loss spectroscopy and can access those resonances formed in electron impact, with the important caveat that the selection rules differ and the initial molecular geometries differ[17]. For $C_6F_6^-$, there are large changes in geometries, causing this complementarity to break down. Nevertheless, as will be discussed below, the 2D PE spectra provide information about resonances accessible from the anion ground state. Our PE spectra of $C_6F_6^-$ are broadly in agreement with the previous studies, although we do not observe the vibrational structure seen by Bowen and coworkers. Moreover, we collect the PE angular distributions and these are also consistent with a Jahn-Teller distorted geometry. We observed the lowest triplet state of C_6F_6 and show that it has bent geometry, similar to that of $C_6F_6^-$. Additionally, there is evidence for resonances in $C_6F_6^-$, which we assign with the aid of electronic structure calculations. Finally, we also show results from $I^-C_6F_6$ in which we excite a charge-transfer band that accesses the non-valence state[9]. The PE spectrum of the non-valence state is tentatively assigned and we analyse the time-resolved conversion from non-valence to valence with the aid of the electronic structure of $C_6F_6^-$ determined from the 2D PE spectra and computational results.

EXPERIMENTAL AND COMPUTATIONAL DETAILS

Anion photoelectron spectrometer

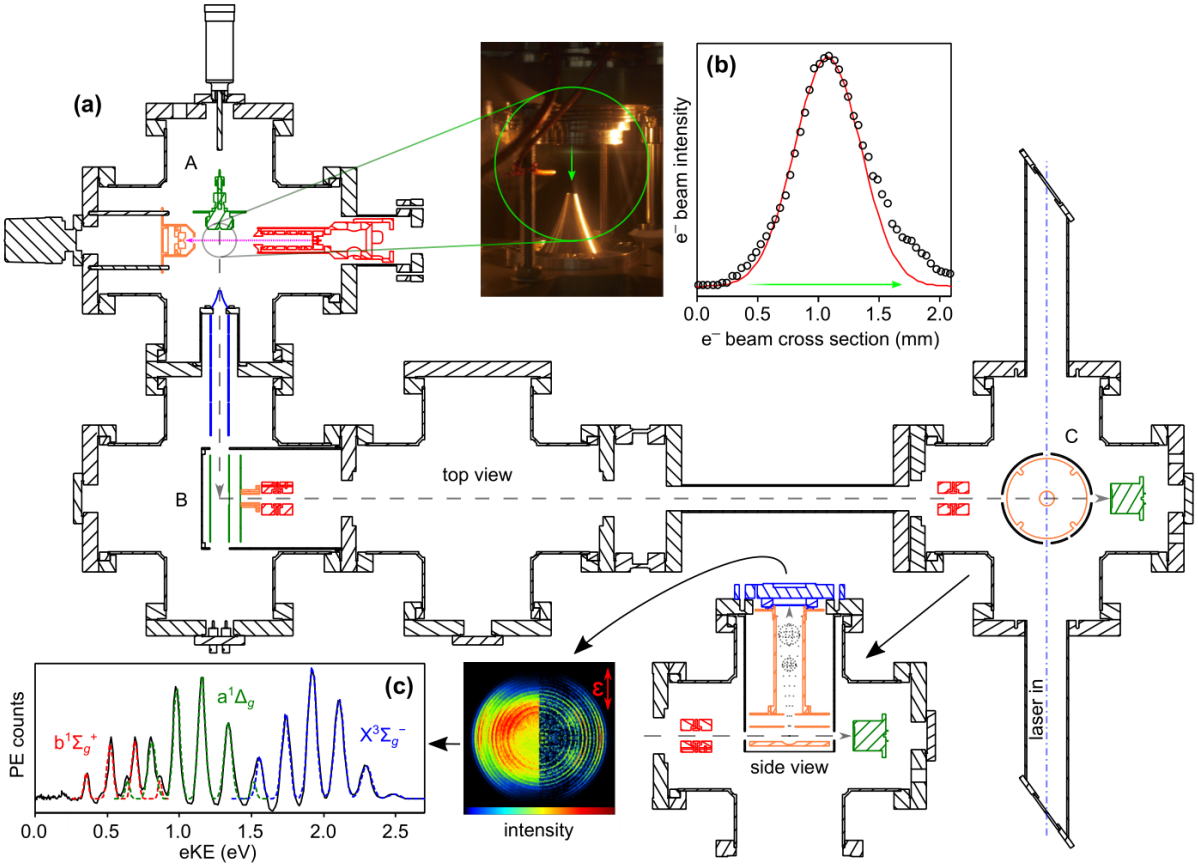

Figure 1: Overview of anion photoelectron imaging instrument. A schematic of the top-view of the instrument is shown in (a) where A is the ion source, B the time-of-flight plates of the mass-spectrometer, and C the velocity map imaging PE spectrometer, which is also shown as a side-view. (b) shows the electron beam profile in the expansion. (c) shows the PE spectrum of O_2^- derived from the PE image with the left half being the raw (2D crushed) PE image and the right half the reconstructed central slice through the 3D PE distribution.

We have recently developed a new anion PE spectrometer, which we will detail here for the first time. An overview of the instrument is shown in Figure 1(a). It consists of molecular beam anion source followed by a time-of-flight (TOF) mass spectrometer coupled to a velocity-map imaging (VMI) PE spectrometer[20]. A supersonic expansion is formed by expanding seeded analyte molecules in a carrier gas using a high temperature Even-Lavie pulsed valve[21]. The expansion is crossed with a focussed electron beam (1 mA beam current

with a full width at half maximum of 0.6 mm and 300 eV kinetic energy – see Figure 1(b)), generated by a home-built electron gun. The location of ionisation within the supersonic expansion is adjustable by translating the valve relative to the fixed electron beam axis. The supersonic expansion passes through a skimmer and a series of tubular collimating electrodes. After travelling 0.38 m, the gas cloud enters a Wiley-McLaren TOF assembly[22], which is rapidly switched to a high negative voltage (<10 ns risetime). The ions are accelerated orthogonally to a kinetic energy of ~ 3 keV and pass through a set of deflectors and an einzel lens that steer and collimate the beam, respectively, down a 1.2 m drift region. The temporal focus of the ion packets is tuned to coincide with the front plate of an ion detector (MCP with scintillator and PMT), enabling the monitoring of TOF mass spectra. The mass-spectrometer has a resolution of $m/\Delta m$ ~ 1500. Immediately prior to this detector is a three-plate VMI PE spectrometer. A laser pulse is timed to intercept the selected mass packet in the interaction volume at the center of the VMI spectrometer. A few nanoseconds prior to the laser pulse arrival, the bottom VMI plate is switched from ground to approximately −480 V and after around 100 ns returns to ground. The middle VMI plate remains static throughout at around −30 V to minimise the possibility of extraneous charges entering the VMI drift region. The top VMI plate is held at +650 V and is in electrical contact with the front of a position sensitive dual microchannel plate detector (Photek VID240). The back of the microchannel plate detector is held at +2.05 kV and the anode of the detector is a phosphor screen held at +6.00 kV. The short switching time in the VMI spectrometer leads to minimal deflection of the molecular ion beam allowing simultaneous monitoring of the PE images and mass spectrum. PE strikes are captured by a charge-coupled device (CCD) camera external to the vacuum system and a heat map is accumulated over many laser shots. The polar onion-peeling algorithm reconstructs the 3D PE distribution and extracts the central slice[23], which

contains the velocity information necessary to produce the PE spectrum and the corresponding PE angular distribution (PAD)[24].

The PE spectrometer was calibrated using the known PE spectrum[25] of O_2^-. Figure 1(c) shows the raw PE image and PE spectrum taken at a photon energy $h\nu$ = 2.95 eV, with peaks corresponding to vibrational progressions in the $X^3\Sigma_g^-$, $a^1\Delta_g$ and $b^1\Sigma_g^+$ electronic states of neutral O_2. The spectral resolution of the instrument is determined to be $\Delta eKE/eKE$ = 2.6 %, where eKE is the electron kinetic energy.

Several components (e.g. spacers, alignment tools, mounts) in the instrument were fabricated from polylactic acid (PLA) using a 3D printer. Even with trapped volumes of air within the bulk of the material, a component with a suitably sealed surface (which may be enhanced by exposing the printed PLA to THF vapour for ~10 s) could achieve base pressures of 1×10^{-9} mbar using a 700 l s^{-1} turbomolecular pump. The 3D printed PLA components themselves did not show any adverse effects of being in vacuum and no significant outgassing was observed. We have not, however, performed a residual gas analysis (RGA) and we note that PLA begins to lose structural rigidity at around 350 K. We have now deployed 3D printed PLA components extensively for in-vacuum components and as a versatile (and cost effective) source of insulators. Osterwalder and coworkers have also electroplated 3D printed components opening the door to using 3D printed conductors[26].

Experimental details

Clusters of C_6F_6, $(C_6F_6)_n^-$, were generated by passing 3.0 ± 0.5 bar Ar over a small reservoir of liquid hexafluorobenzene and expanding into vacuum at an operating pressure of ~10^{-5} mbar. For the production of $I^-C_6F_6$, a small amount of CF_3I was seeded into the Ar carrier gas. The expansion was crossed with the electron beam ~ 2 mm from the throat of the expansion. A typical TOF mass spectrum is shown in Figure 2, which also shows trace

amounts of O_2 and H_2O that were present for calibration reasons. A Nd:YAG pumped tuneable pulsed OPO laser delivered optical pulses polarised parallel to the plane of the position-sensitive photoelectron detector. Pulses were of ~5 ns duration in the range $1.8 \leq h\nu \leq 5.8$ eV with a linewidth of <10 cm^{-1}. The repetition rate of the experiment was 10 Hz and the acquisition time for each spectrum was varied from between 10 s to 30 min depending on the number of ions in the primary beam and the power of the laser at the desired wavelength. There is a minimum in the OPO output around $h\nu$ = 3.10 eV. Background images (no ion beam present) were acquired and subtracted from the PE spectra for $h\nu$ > 4.8 eV to remove PE noise when using UV light.

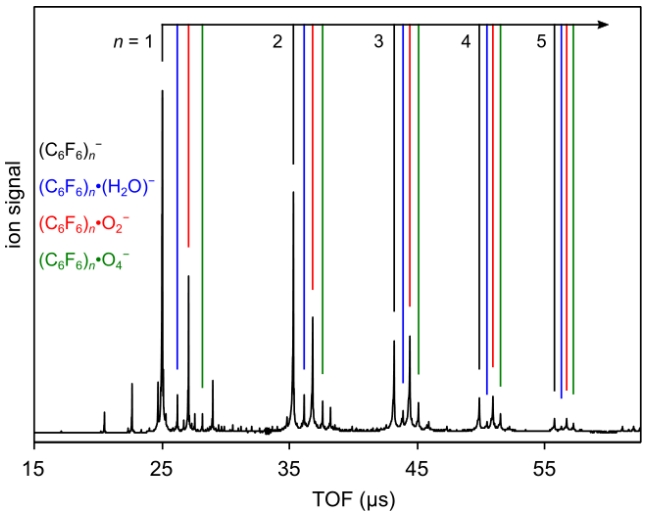

Figure 2: Time-of-flight mass spectrum of $(C_6F_6)_n^-$ and other clusters used to calibrate the mass spectrometer.

C. Computational details

Electronic structure calculations were performed using the Gaussian 09 computational package[27]. Initial optimizations of the anion and neutral ground state geometries were carried out using density functional theory (DFT), with the CAM-B3LYP functional[28] and the aug-cc-pVDZ Dunning basis set[29], both chosen due to their acceptable treatment of anions. The

geometries were confirmed to represent the global energetic minima through vibrational frequency analysis. Exploration of excited states of the anion and neutral were undertaken using linear-response time-dependent (LR-TD) DFT calculations[30-32], with the Tamm-Dancoff approximation[33] and the same functional and basis set as ground state calculations. The results of these calculations were used to confirm both the character and energetics of excited states accessed experimentally. Additional LR-TDDFT calculations were performed to investigate the minimum energy geometries of the first two triplet states.

Details of the calculations on the $I^-C_6F_6$ cluster have been reported previously[9]. Geometric displacements along the vibrational mode attributed to coupling the ground state geometries of the anion and neutral C_6F_6 at 120 cm^{-1} were sampled using Avogadro software[34] Version 1.2.0. LR-TDDFT calculations investigated the changing potential energy surface landscapes of excited states of $C_6F_6^-$ as a function of this displacement. These LR-TDDFT calculations used the same level of theory as detailed above.

RESULTS AND DISCUSSION

C_6F_6 anion and neutral states

Figure 3 shows the 2D-PE spectrum of $C_6F_6^-$ acquired in the range 1.8 eV ≤ $h\nu$ ≤ 5.8 eV in steps of 0.1 eV as a false colour plot in which the PE spectra have been normalised to their total integrated PE signal. Representative PE spectra are shown in Figure 4 with (a) $h\nu$ = 2.5 eV, (b) $h\nu$ = 4.5 eV, and (c) $h\nu$ = 5.5 eV. Figure 4(a) also shows the PE spectrum ($h\nu$ = 2.5 eV) on a log scale (red data points). Figure 4(d) shows the raw PE image at $h\nu$ = 2.5 eV. The PE image indicates that the emission is very anisotropic, peaking along the polarisation axis.

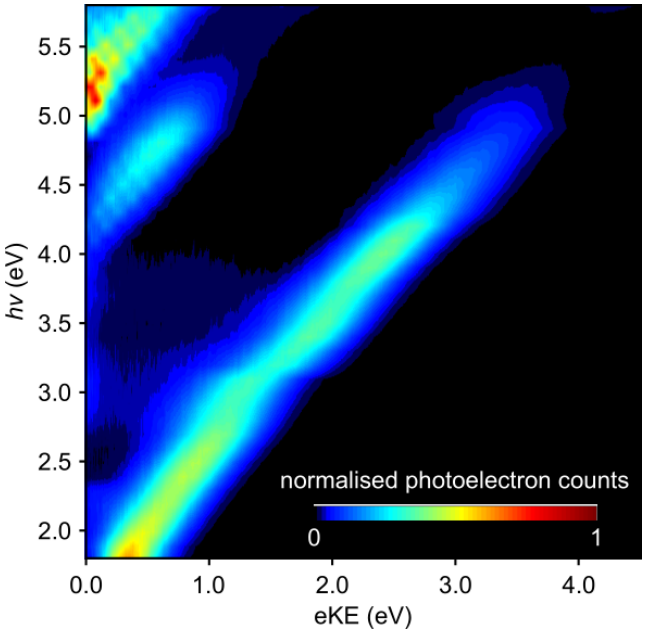

Figure 3: 2D Photoelectron (PE) spectrum of $C_6F_6^-$ in the range 1.8 ≤ $h\nu$ ≤ 5.8 eV at intervals of 0.1 eV. Each PE spectrum has been normalised to its total integrated signal.

The 2D-PE spectrum in Figure 3 show that the peak at highest eKE increases by an amount equal to the increase in $h\nu$, indicating that this feature corresponds to a direct detachment process[17]. The maximum of this peak has an electron binding energy, eBE = $h\nu$ – eKE, defined as the vertical detachment energy (VDE). From the data, we determined to be

VDE = 1.60±0.07 eV. Figure 4(a) shows that the feature is broad with a Gaussian profile (the blue line fitted to the log plot is quadratic). Such a profile is expected when the geometries of the anion and neutral differ significantly and the Franck-Condon profile is substantially shifted away from the 0-0 transition.

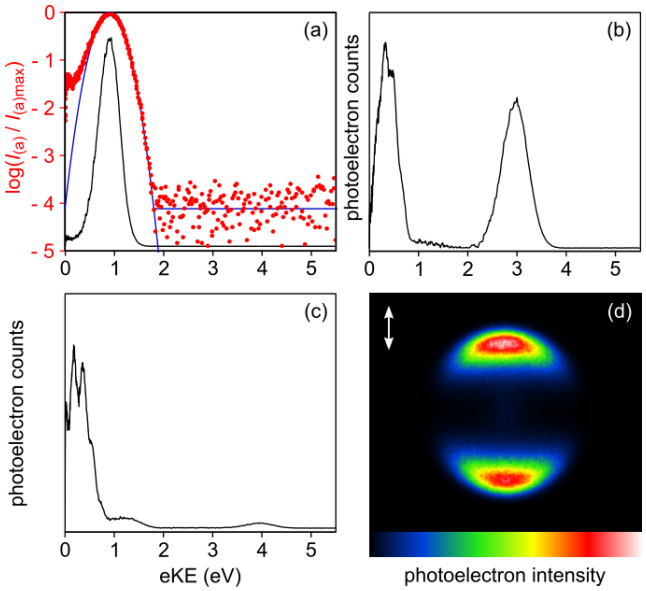

Figure 4: Representative photoelectron (PE) data for $C_6F_6^-$. PE spectra (black lines) taken at $h\nu$ = 2.5 eV (a), 4.5 eV (b), and 5.5 eV (c). The raw PE image for $h\nu$ = 2.5 eV is shown in (d), where the vertical double arrow indicates the polarisation axis of the light. A log plot of the PE signal for $h\nu$ = 2.5 eV is also shown in (a) (red data points), along with a fit (solid blue line) to a parabola.

Figure 5(a) and (b) show the minimum energy structures of C_6F_6 and $C_6F_6^-$, along with the highest-occupied (HO) molecular orbital (MO) and singly-occupied MO (SOMO), respectively. The buckled geometry is a consequence of a Jahn-Teller and pseudo-Jahn-Teller distortion because of the SOMO and leads to a C_{2v} structure. The SOMO is predominantly of σ* character such that the emitted PE wave is almost a pure p-wave[35], resulting in a PAD peaking along the polarisation axis. This is consistent with the PE image in Figure 4(d).

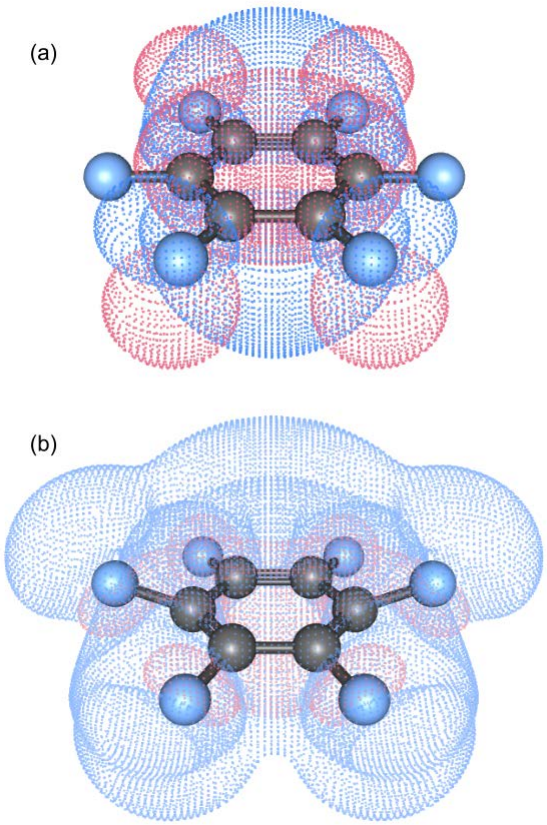

Figure 5: Minimum energy geometries of C_6F_6 (a) and $C_6F_6^-$ (b), along with the highest-occupied (HO) molecular orbital (MO) and singly-occupied (SOMO),

The differing anion and neutral geometries preclude the direct observation of the 0-0 transition and, by extension, the experimental determination of the adiabatic detachment energy (ADE). From Figure 4(a), the signal-to-noise ratio is approximately 40 dB. The blue lines indicate where the noise baseline meets a parabolic fit that arises from the Gaussian profile of the peak. From this intersection we can conclude that ADE ≤ 0.70 eV. We quote this here as a maximum value because the fit suggests that the 0-0 transition is not probed directly in the experiment. The measured ADE is in agreement with previous computational work[4-6] and our own electronic structure calculations which predict ADE = 0.55 eV. Similarly, the calculated VDE = 1.70 eV is in agreement with experiment at 1.60±0.07 eV.

Figure 6 shows an energy level diagram with the relative energies of the $C_6F_6^-$ and C_6F_6 in the anion and neutral geometries, along with calculated excited states of $C_6F_6^-$ and C_6F_6.

The above PE spectroscopic results are consistent with those presented previously by the Kaya and Bowen groups[15-16]. However, we do not reproduce the sharp vibrational structure observed by the Bowen group. In principle, our resolution should be sufficient to observe this structure. Moreover, it is not immediately clear where such vibrational structure should come from because vertical photodetachment from the anion accesses a steep part of the neutral potential energy surface suggesting a very high density of vibrational states would be encompassed in the Franck-Condon window

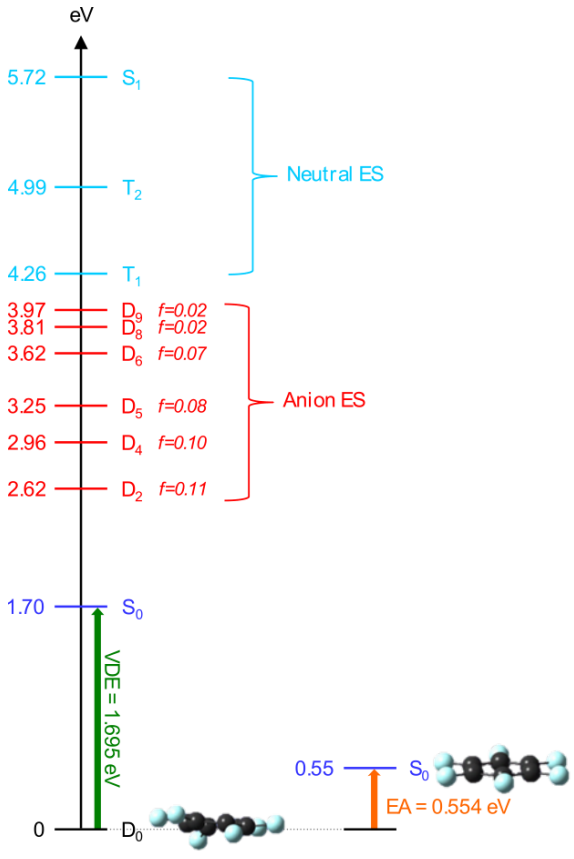

Figure 6: Calculated energy level diagram of the ground (black) and doublet excited states (red) of $C_6F_6^-$ that have a significant oscillator strength, and ground (blue) and excited states (magenta) of C_6F_6 in the anion geometry. The relative energy of the ground state in the neutral geometry is indicated.

Figure 3 shows the appearance of two additional direct detachment features at lower eKE (higher eBE) for $h\nu > 5$ eV. These are presented more clearly in Figures 4(b) and (c). Both PE features show vibrational structure. According to our electronic structure calculations (Figure 6), these features correspond to the two lowest triplet states of the C_6F_6, T_1 and T_2. From the PE spectra, we find that the adiabatic energy of the T_1 and T_2 states relative to the anion ground state to be 3.73±0.10 and 4.70±0.10 eV, respectively. This compares reasonably well with their calculated energies at 4.26 and 4.99 eV, respectively. The fact that vibrational structure is observed, especially for the T_2 excited state, points to a comparatively small geometric difference between the two lowest triplet states and the anion buckled geometry (shown in Figure 5(b)). Indeed, our calculations show that the lowest energy structures for T_1 and T_2 have buckled geometries. Note that the S_1 state of neutral C_6F_6 is calculated to lie at 5.72 eV above the anion so that it is not seen in our experiment.

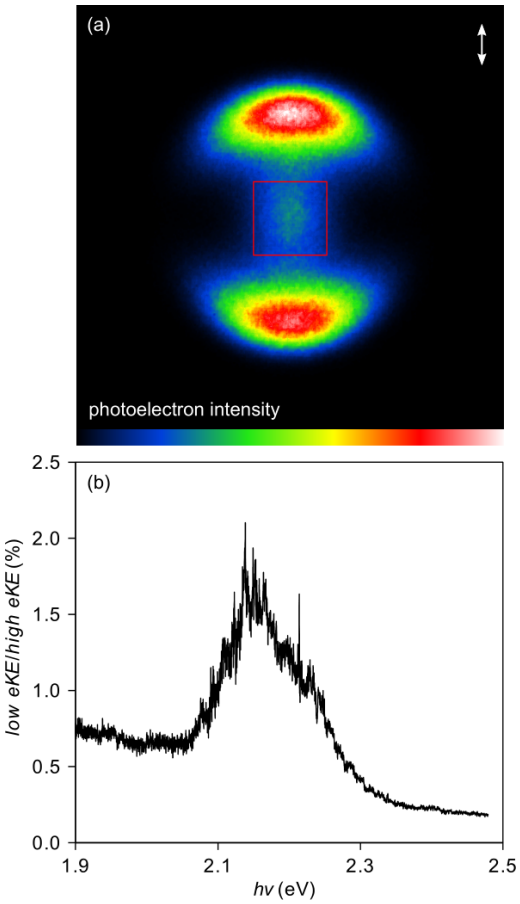

Figure 7: (a) PE image of $C_6F_6^-$ taken at $h\nu$ = 2.2 eV showing direct and indirect (boxed in the centre of image) detachment channels. Vertical double arrow indicates the polarisation axis of the light. (b) Action spectrum acquired by taking the ratio of indirect to direct detachment channels as a function of $h\nu$.

In addition to the direct detachment channels ($S_0 + e^-$, $T_1 + e^-$, and $T_2 + e^-$), there is also evidence in the 2D-PE spectra that excited states (resonances) of $C_6F_6^-$ are excited. This can be seen in around $h\nu$ = 3.0 eV and for $h\nu$ < 2.4 eV. In the latter range, very low energy electrons are emitted, which can be appreciated from the raw PE image taken at $h\nu$ = 2.2 eV shown in Figure 7(a). As the direct photodetachment channel is strongly anisotropic and predominantly of p-wave character, very few electrons should be emitted at threshold because of the threshold behaviour of photodetachment[36]. Yet, the PE image in Figure 7(a) shows some isotropic emission near threshold suggesting that there is a detachment process accessible via an indirect mechanism. We have crudely analysed the absorption (action)

spectrum associated with the appearance of these low energy electrons by integrating the central area of the image (indicated in Figure 7(a) by a box) as a fraction of the total PE counts in the image. The results of this analysis are shown in Figure 7(b) over the range $1.9 < h\nu < 2.5$ eV. The rising background towards lower $h\nu$ is an experimental artefact that comes about from the fact that the PE signal in the direct detachment peak overlaps more with the boxed region of the image in Figure 7(a) at lower $h\nu$. Figure 7(b) shows a broad structureless peak centred at $h\nu \sim 2.2$ eV. The relative contribution of the indirect feature is in fact quite small, amounting to only ~ 1% of the direct PE signal. According to our calculations, the D_1 excited state lies at 2.36 eV above the D_0 (in the anion geometry) and could be a candidate for this resonance. While this transition has negligible oscillator strength at the optimised anion geometry on symmetry grounds (and was therefore not included in Figure 6), our calculations also show that it gains significant oscillator strength with small geometric perturbations of the lowest frequency modes. Therefore, this transition may be observed and the intensity seen in Figure 7(b) is consistent with the calculated small oscillator strength.

Additional evidence for resonance dynamics can be seen between $2.7 < h\nu < 3.9$ eV, where PE signal is observed at lower eKE than that of the direct $S_0 + e^-$ channel. A representative PE spectrum at $h\nu = 2.9$ eV is shown in Figure 8. According to our calculations (Figure 6), there are several candidate resonances; there are three optically bright doublet states between 2.62 and 3.25 eV. The appearance of electrons at lower eKE most likely arises from nuclear motion on the potential energy surface of the resonance that leads to changes in the Franck-Condon overlap with the neutral ground state. This has been seen in several PE spectroscopic studies[37-42]. We also note that the direct detachment peak appears slightly shifted towards lower eKE, which again points to the presence of resonances[43]. We cannot identify which of the three bright resonances contribute to the spectral changes, but it

is clear that above-threshold dynamics are occurring that lead to electron emission at lower eKE.

The location of resonances of $C_6F_6^-$ have been studied using electron impact spectroscopy[7]. However, these are of limited use as a comparison to the current study because of the large structural difference between the initial geometries of the anion and neutral species.

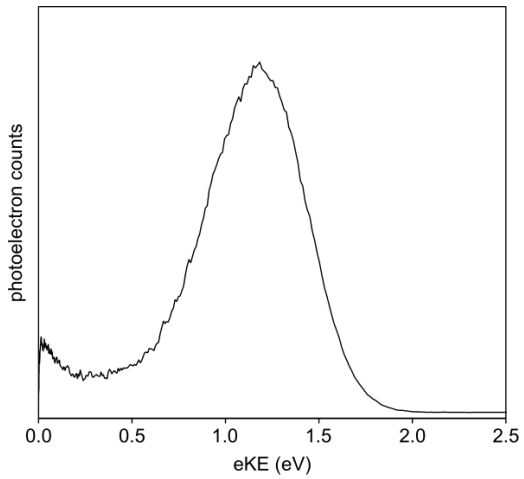

Figure 8: PE spectrum of $C_6F_6^-$ taken at $h\nu$ = 2.9 eV. Signal at eKE < 0.5 eV arises from indirect detachment following excitation to resonances.

Finally, we briefly comment on the apparent change in slope of the direct detachment channel leading to the S_0 state around $h\nu \sim 3$ eV. Firstly, because of the resonances around 3 eV, the shape of the "direct" detachment also includes contributions from some indirect electron emission, which pushes the apparent VDE to lower eKE. Secondly, because of the width of the direct peak is so large, as $h\nu$ becomes smaller, part of the peak is below threshold, which (because of the threshold behaviour) has the appearance of pushing the VDE to higher energy. Finally, it is also worth noting that the output of the OPO reaches a minimum at 3.10 eV so that there is increased noise at this $h\nu$.

C_6F_6 anion clusters, $(C_6F_6)_n^-$

Figure 9 shows the 2D-PE spectra for $(C_6F_6)_2^-$. Overall, these data appear similar to the 2D-PE spectra in Figure 3. Specifically, the same direct detachment channels ($S_0 + e^-$, $T_1 + e^-$, and $T_2 + e^-$) are present, although the vibrational structure in the triplet neutral states is less apparent. Additionally, the onset of the direct detachment channels has increased by ~200 meV compared to the unclustered $C_6F_6^-$ ion. This increase in VDE (and ADE) predominantly arises from the cohesion energy of the cluster.

In addition to the direct detachment channels, there is again evidence of resonance dynamics occurring that leads to electron emission at lower eKE than expected for the direct $S_0 + e^-$ channel. The range over which such emission is observed is broader in the dimer than in the monomer PE spectrum; weak signal occurs at most measured *hv*, with particularly clear evidence for resonance dynamics in the regions of *hv* ~ 2.8, 3.7, and 4.3 eV. We have not performed detailed calculations of the excited state $(C_6F_6)_2^-$ and offer no assignment of the electronic states facilitating these dynamics.

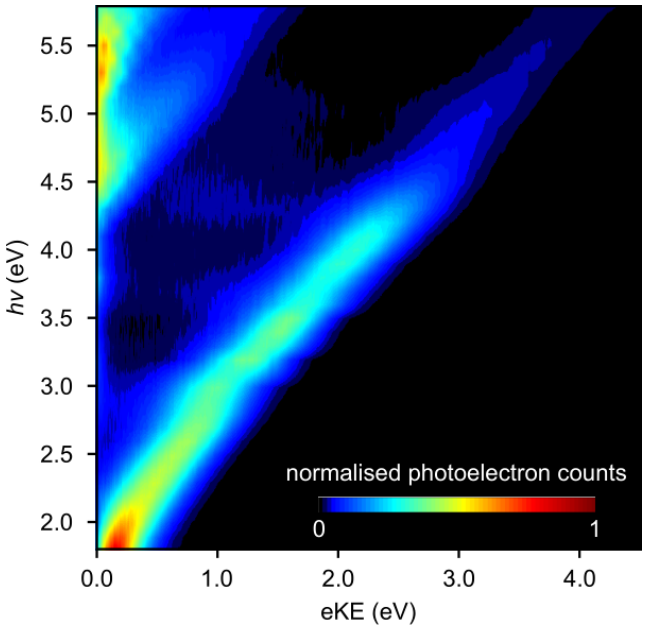

Figure 9: 2D PE spectra of $(C_6F_6)_2^-$ in the range $1.8 \leq hv \leq 5.8$ eV at intervals of 0.1 eV. Each PE spectrum has been normalised to its total integrated signal.

For $h\nu$ > 4.2 eV, there appears to be enhanced signal at very low eKE. Such electrons are indicative of a delayed emission process in which the emission is becoming more statistical in nature, again pointing to dynamics involving resonances[17]. However, this delayed emission channel coincides with the opening of the $T_1 + e^-$ and $T_2 + e^-$ detachment channels. We have previously considered the origin of this signal and assigned it to an indirect mechanism in which the outgoing PE is captured by the non-valence anion state localised on the solvent molecule[10]. A similar onset of the appearance of low-eKE electrons at the opening of the $T_1 + e^-$ and $T_2 + e^-$ detachment channels was also observed for large clusters (with up to 5 molecules), suggesting a common mechanism in all clusters, which would be consistent with a picture in which the low-eKE outgoing electron is recaptured by a solvent molecule.

Figure 10 shows a series of PE spectra for $(C_6F_6)_n^-$ taken at $h\nu$ = 3.80 eV, which clearly show that an incremental increase in cluster size leads to an increase in the VDE. In Figure 11, the measured increase in VDE is plotted as a function of cluster size, n. This shows a roughly linear trend with a gradient of 200 ± 20 meV n^{-1}, indicating that photoemission occurs from $C_6F_6^-$ solvated in a C_6F_6 cluster: $C_6F_6^-(C_6F_6)_{n-1}$. This is consistent with the observation that for all $(C_6F_6)_n^-$, the direct $S_0 + e^-$ photodetachment is highly anisotropic peaking along the polarisation axis. We conclude therefore that the emitted PE originates from the SOMO of $C_6F_6^-$ (Figure 5), which, although energetically stabilised, is not substantially perturbed by the surrounding solvent cluster.

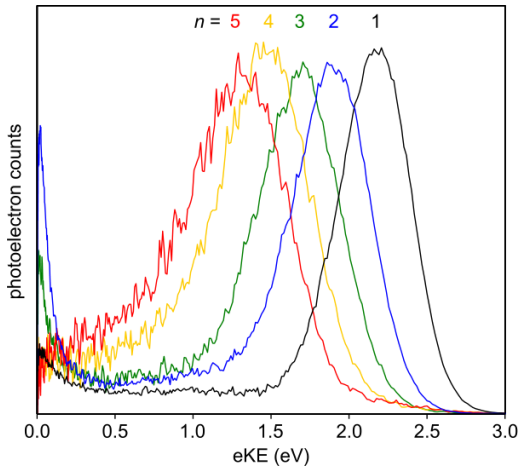

Figure 10: PE spectra of $(C_6F_6)_n^-$ (n = 1-5) taken at $h\nu$ = 3.80 eV

The observed increase in VDE as a function of n is in agreement with that of Nakajima *et al.*[16] over the same range (up to n = 5) as shown in Figure 11. Our data and that of Nakajima *et al.* suggests that the increase in VDE up to n = 5 is essentially linear. Beyond this range (up to n = 8), Nakajima *et al.* showed the incremental increase becomes smaller (see Figure 11). It is also interesting to note that the FWHM of the direct detachment peaks in Figure 10 appears to grow with increasing n. Although this trend is not seen in the measurements made by Nakajima *et al.*, a direct comparison may not be appropriate because the two experiments were not performed at the same excitation energy and resonances may affect the apparent width of these features.

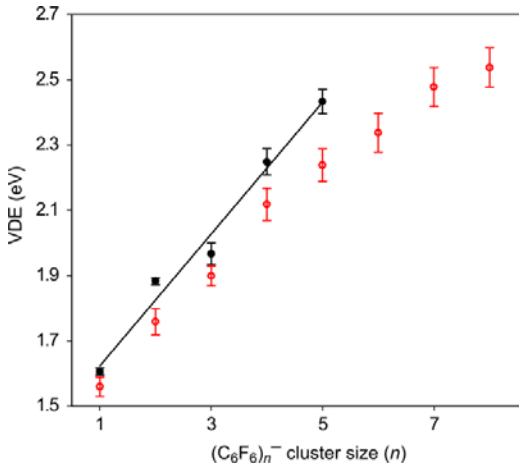

Figure 11: Measured vertical detachment energies (VDE) for $(C_6F_6)_n^-$ for n = 1-5 from the present study (black full circles) with a linear fit (sold line), and with n = 1-8 from Nakajima *et al.*[16] (red open circles).

$I^-C_6F_6$ cluster: Photoelectron and photodetachment spectroscopy

The 2D-PE spectrum of $I^-(C_6F_6)$ has been presented previously[9]. In brief, this data showed that the charge is localised on the iodide and direct detachment essentially yields the PE spectrum of I^-, shifted to higher eBE by the cluster binding energy with C_6F_6. Hence, the $I^-(C_6F_6)$ complex can be viewed as I^- solvated by a neutral (planar) C_6F_6 molecule. Below the adiabatic detachment energy, PE signal was observed and assigned to detachment from I^-. Such signal can only arise from the excitation of the $I^-(C_6F_6)$ complex to some excited state that then dissociates to yield I^- and a second photon within the ~5 ns pulse detaches an electron leading to the observed PE spectrum of I^-. The excited state is a charge-transfer state, which injects the electron onto the planar C_6F_6. In principle, an action spectrum of this absorption band could be measured by monitoring the I^- yield as a function of *hv*. However, we do not have the ability to measure secondary mass spectra in our current experiment. Instead, we have monitored the total electron yield as a function of *hv*. The electron yield following excitation of $I^-(C_6F_6)$ below the ADE is expected to depend quadratically on the

laser intensity because of the two-photon (sequential) process. In Figure 12, the photodetachment action spectrum (square-root of total electron yield) is shown in the range $3.1 < h\nu < 3.5$ eV. This spectrum clearly shows a peak around $h\nu \sim 3.3$ eV, below the ADE of the direct detachment channel (ADE = 3.48 eV) [9]. We note, however, that the 355 nm pumped OPO is unstable around $h\nu = 3.1$ eV such that the rising edge of this was difficult to acquire confidently. Any apparent structure in the band is mostly noise.

In order to confirm the measurement of an action spectrum below the onset of the $I[^2P_{3/2}]\cdot C_6F_6 + e^-$ channel, we have also acquired a low resolution action spectrum just below the onset of the second $I[^2P_{1/2}]\cdot C_6F_6 + e^-$ channel. Substantial low eKE PE signal was observed in the 2D-PE spectra in this range indicating an indirect electron loss mechanism, which in turn implies the presence a resonant excited state[9]. In order to determine the spectral shape of its absorption band, we performed the same analysis on these spectra as in Figure 7, comparing the yield of low eKE electrons to the PE signal arising from the direct detachment process. This ratio is represented by the red circles in Figure 12. The overall peak shape of the two action spectra match but are offset by 0.94 eV, in agreement with the spin-orbit splitting in iodine. Although neither method is ideally suited to record an action spectrum, there is adequate qualitative agreement over the shape and location of the absorption bands.

The peak of the absorption is ~0.2 eV below the opening of the respective detachment channels, suggesting that the excited state is bound by this amount. However, we also note that the peaks are broad and have a width of ~0.2 eV (full width at half maximum). It is not immediately clear why the absorption band should be this broad. Nevertheless, similar broad absorption bands have been seen in the action spectra of iodide with pyrrole[44]. In our time-resolved experiments (described below), the red-edge of the absorption band was excited with $h\nu = 3.10$ eV.

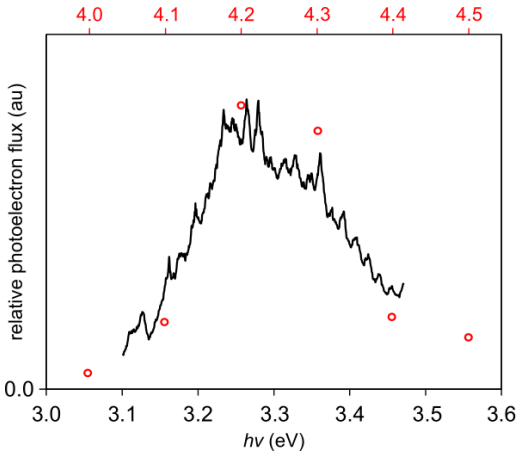

Figure 12: Action (absorption) spectra of $I^-(C_6F_6)$ near the $I[^2P_{3/2}]\cdot C_6F_6 + e^-$ channel (solid black line) and the $I[^2P_{1/2}]\cdot C_6F_6 + e^-$ channel (open red circles). Solid black line is acquired by monitoring the total PE yield as a function of *hv*. The signal has been square rooted to account for the 2-photon nature of this feature. The red data points are acquired by taking the ratio of very low energy (indirect detachment) photoelectrons to high energy (direct detachment) photoelectrons.

$I^-C_6F_6$ cluster: Ultrafast dynamics following charge-transfer

The dynamics following excitation of the charge-transfer band just below the $I[^2P_{3/2}]\cdot C_6F_6 + e^-$ channel were probed by time-resolved photoelectron imaging[9] (pump at 3.10 eV and probe at 1.55 eV) and the results have been reproduced here in Figure 13(a). Briefly, the peak at high eKE and at $t = 0$ was assigned to the formation of a transient non-valence state of $C_6F_6^-$. This non-valence state then evolves on a 30 fs timescale to the valence state of $C_6F_6^-$ (see Figure 5(b)). The oscillatory motion observed in the time-resolved PE spectra represents the buckling motion of $C_6F_6^-$ as it evolves from the planar geometry (associated with the non-valence state) to the buckled geometry (associated with the ground valence state – Figure 5). These dynamics could be conveniently tracked by integration over spectral ranges (highlighted in Figure 13(a)), as shown in Figure 13(b).

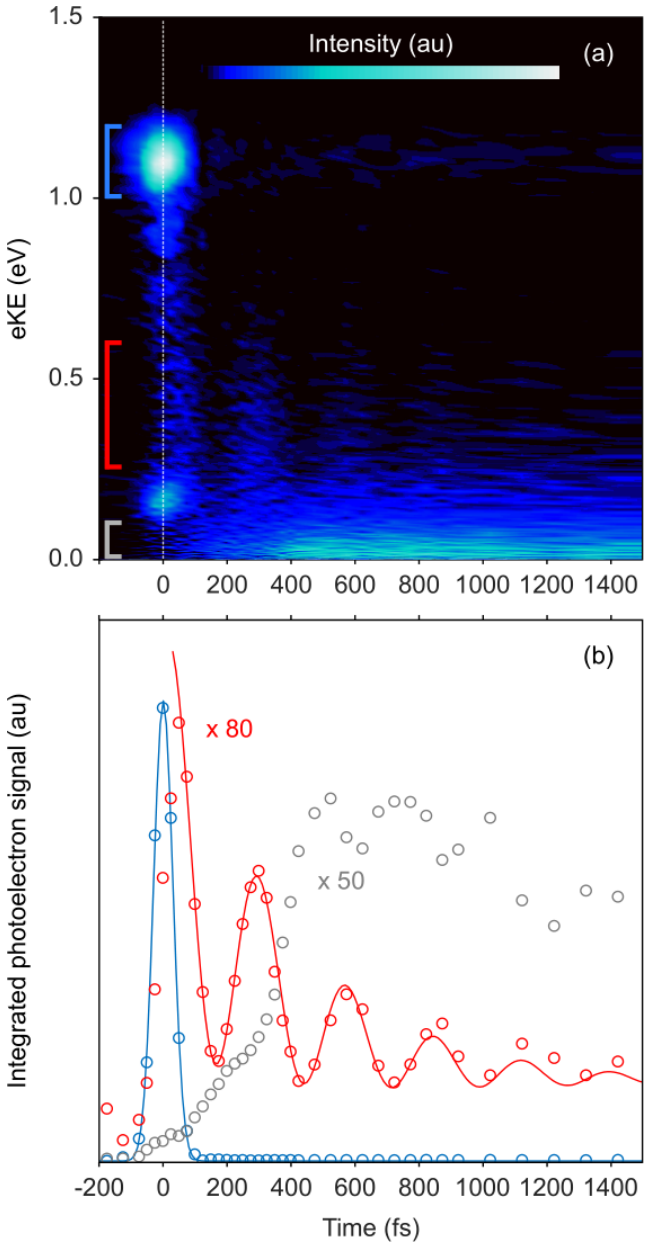

Figure 13: (a) Time-resolved PE spectra of $I^{-}\cdot(C_6F_6)$ excited at 3.10 and probed at 1.55 eV. *t* = 0 is indicated by a vertical dashed line. (b) Integrated photoelectron signal (open circles) over spectral windows indicated by the correspondingly coloured square brackets in (a). A fit to the oscillatory signal is included. This figure has been reproduced from reference 9.

Although the energy difference between the neutral and anion states in the planar geometry is small, our calculations show that this energy difference increases rapidly as the buckling angle increases. The energy difference can be attributed to a reduction in the energy

of the anion as well as an increase in the energy of the neutral. From our $C_6F_6^-$ PE spectra, the difference between the anion and neutral at the anion valence state minimum is VDE = 1.60 eV (ignoring the presence of the iodine). At this point, some PE signal will still be observable based on a 1.55 eV probe and the width of the direct detachment peak (Figure 4). Experimentally, however, Figure 13(a) shows that the PE signal essentially disappears for eKE > 0.2 eV. This can be rationalised because the coherent motion naturally leads the molecule to buckle beyond its minimum energy geometry. While the anion state energy must increase, our calculations show that the corresponding neutral state energy is increasing more rapidly and therefore, the eKE measured by photodetachment with the probe decreases. Hence, the minimum of the pump-probe PE signal corresponds to a maximal buckling angle. Note that the above is based solely on energetic arguments and omits that the detachment cross-section along the buckling mode may also change.

A specific (dominant) vibrational mode of e_{2u} symmetry was assigned to the motion which has a calculated frequency (120 cm^{-1}) that matches the measured beat frequency (121±2 cm^{-1}). As part of the present study, we performed calculations in which we displaced the atoms along this vibrational mode vector (starting from the valence anionic minimum energy geometry). The results of this are shown in Figure 14 and indicate that the potential energy surface along this mode is mostly harmonic, consistent with the observed wavepacket motion in Figure 13.

In addition to the oscillatory signal in Figure 13, dynamics can also be seen in the low eKE spectral range (eKE < 0.2 eV), which were not previously discussed. This low eKE peak has the appearance of an indirect detachment process and does not change in shape with pump-probe delay. This low eKE feature is not present in the single colour 3.10 eV PE spectrum and we therefore infer that the source of this low eKE peak must be a consequence of the interaction with the probe pulse. Its dynamics (integrated over 0.0 < eKE < 0.1 eV)

show a step-like increase in the yield (see Figure 13(b)) and these steps are nearly π out-of-phase with the oscillatory dynamics observed in the 0.25 < eKE < 0.60 eV spectral window.

Given that a probe photon is required for the production of the low eKE PE signal and that it appears to be an indirect process, we consider if excited states of $C_6F_6^-$ may be accessed by the probe photon. Figure 6 showed that resonances are available in $C_6F_6^-$. However, the energy of these resonances is based on $C_6F_6^-$ in its minimum energy geometry, while the dynamics access a wide range of buckle angles. We therefore considered the excited states of $C_6F_6^-$ at geometries away from the equilibrium of the valence state anion. Specifically, we calculated the excited states accessible at each geometry along the vibrational mode as shown in Figure 14. In the minimum energy geometry of the valence anion, the lowest energy bright transition involves a SOMO → LUMO excitation to the D_2 excited state. The energy of this transition is > 2 eV and increases with greater buckle angle and is thus inaccessible the 1.55 eV probe. In contrast, the excited state corresponding to the excitation from HOMO → SOMO (D_5 excited state in Figure 6), which is at > 3 eV at the minimum energy geometry, rapidly decreases in energy with a greater distortion along the vibrational buckling mode. While our calculations have not sampled the vibrational coordinate very accurately to predict the relevant energy profile of this excited state exactly, the trend is clear. As the molecule nears outer turning point, the transition energy to this state decreases. Hence, it seems reasonable to consider that near the outer turning point of the motion, the probe pulse may access this excited state. Note that at the extreme geometry, the excited state is bound (vertically) relative to the neutral and so the electron cannot detach directly. However, adiabatically, the excited state is unbound and we speculate that accessing this excited state eventually leads to autodetachment that produces the low eKE electrons observed in Figure 13.

The above interpretation considered a simplified one-dimensional picture, lacking consideration of other vibrational modes that might be important, especially at the large geometric distortions in the extremes of the 1D cut along the buckling coordinate. The coupling to other modes is consistent with the dephasing of the wavepacket in Figure 13(a). It thus appears that, as other vibrational modes are populated along the buckling motion, the width of the transition increases and other electronic transitions become available along the entire coordinate, which would lead to the observed step-like signal. After a few vibrations along the buckling coordinate, it appears that much of the vibrational energy has redistributed into these unspecified modes, in agreement with the oscillatory motion in the 0.25 < eKE < 0.60 eV spectral window.

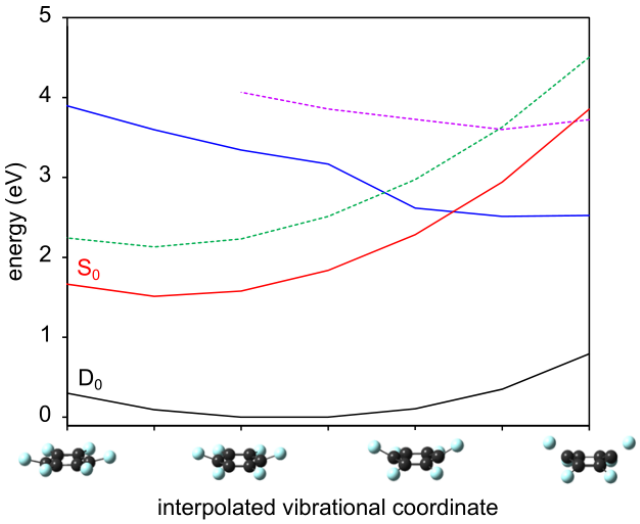

Figure 14: Potential energy curves along the vibrational coordinate of the wavepacket motion of $C_6F_6^-$. The ground electronic states of $C_6F_6^-$ (D_0 black) and C_6F_6 (S_0 red) are shown as well as three excited states of $C_6F_6^-$. The D_2 excited state (green dashed) in the minimum energy geometry of $C_6F_6^-$ increases with buckle angle, while the D_5 excited state (blue solid) decreases so that the probe may become resonant with a transition from D_0 to this excited state. A third (D_9) excited state is included (purple dashed), but probably plays no role in the measured dynamics.

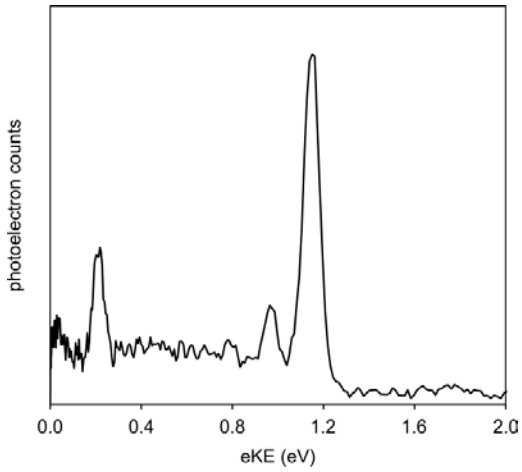

Figure 15: Time-resolved PE spectrum of $I^-(C_6F_6)$ taken at $t = 0$ with a 3.10 eV pump and 1.55 eV probe pulse. This spectrum is effectively the PE spectrum of the non-valence correlation-bound state of the $(C_6F_6)^-$.

$I{\cdot}C_6F_6^-$: Non-valence state photoelectron and photodetachment spectra

We now return to the earliest dynamics following photoexcitation of $I^-(C_6F_6)$ at $h\nu$ = 3.10 eV. A PE spectrum at $t = 0$ (equivalent to a vertical slice in Figure 13(a) at $t = 0$) is shown in Figure 15. This particular PE spectrum was acquired to achieve the best possible signal-to-noise ratio at $t = 0$. The PE spectrum shows an intense peak at eKE = 1.10 eV, which we have previously assigned to the non-valence state of $C_6F_6^-$. There is also a clear peak at eKE = 0.16 eV, offset from the primary peak by the spin-orbit splitting of iodine. This peak may be assigned to a small contribution of detachment from the non-valence state (that is associated with the $^2P_{3/2}$ state of I in $I{\cdot}C_6F_6^-$) to the higher-lying $^2P_{1/2}$ state of I in $I{\cdot}C_6F_6^-$. There is a broad continuum of electrons between the two peaks due to rapid evolution of the non-valence to valence evolution within the finite time-resolution of the experiment[9].

Interestingly, there is a weak progression of peaks on the low eKE side of the peak assigned to direct detachment from the non-valence state. The first of these small peaks is

shifted from the primary peak by 0.18 eV (~1,450 cm^{-1}). The PE spectra of the CH_3CN^- dipole-bound anion measured by Bailey and coworkers exhibited similar vibrational structure[45]. These were assigned to vibrational bands that arise not only from differences in anion and neutral potential energy surfaces, but also from vibrational modes of the neutral that are strongly coupled to the non-valence state. In the case of the dipole-bound state in CH_3CN^-, these distinct peaks arise from the IR active modes because IR modes change the dipole-moment of the molecular core and therefore also the binding of the dipole-bound state. Bailey and coworkers were able to assign the individual peak offsets to particular IR-active vibrational modes of neutral CH_3CN.

We performed a similar analysis on the peaks observed in Figure 15 to ascertain whether they are likely to arise from a similar mechanism in which vibrational modes of C_6F_6 couple to the non-valence state. As the non-valence state of $C_6F_6^-$ is not dipole-bound but predominantly correlation-bound, we may naturally expect that the vibrational modes likely to be strongly coupled to the non-valence state are those that change the molecule's polarizability. However, there is also a contribution from quadrupole-electron interaction in $C_6F_6^-$ and so changes in quadrupole moment may also influence non-valence state binding. Both of these physical properties are affected by Raman active modes. Furthermore, if C_6F_6 distorts to produce a dipole-moment, then there would also be an attractive dipole-electron interaction. Therefore, all Raman and IR active vibrational modes could couple to the non-valence state binding and might be responsible for the spectral features in Figure 15.

The vibrational band (shifted by ~1,450 cm^{-1} from the direct detachment peak from the non-valence state) is close to both the 1,490 cm^{-1} Raman active a_{1g} mode and the bright IR active 1,530 cm^{-1} e_{1u} mode of planar (D_{6h}) C_6F_6[46]. Calculated vibrational modes of C_6F_6 and of $I{\cdot}C_6F_6$ suggest, show that C_6F_6 clustering to iodine, red-shifts the a_{1g} mode and the e_{1u} modes by 30 cm^{-1} and 20 cm^{-1}, respectively. Hence, both modes are very close to the

measured peak shift. Unfortunately, it is not possible to establish whether either or both is observed in the experiment. There is also evidence for a second peak, shifted from the primary peak by twice the frequency of the first, 0.36 eV (~2,900 cm^{-1}). This peak is probably an overtone of the a_{1g} and/or e_{1u} mode because C_6F_6 has no fundamental frequencies of this magnitude. Furthermore, we note that a peak at twice the frequency of the main vibration was also observed by Bailey *et al*. in the CH_3CN^- dipole-bound anion. Although they assigned them to IR modes of the neutral, it is also possible they are overtones of the main peaks (ν_3 and ν_6).

SUMMARY

In summary, a new anion PE imaging instrument is described and used to probe the PE spectroscopy of $(C_6F_6)_n^-$ (n = 1 – 5) over a large photon energy range. The PE images of the monomer showed that the PE emission is highly anisotropic for the $D_0 + h\nu \rightarrow S_0 + e^-$ detachment channel, consistent with the electronic structure of the bent C_{2v} geometry of $C_6F_6^-$. We measure the VDE to be 1.60±0.07 eV and determined the upper limit for the ADE ≤ 0.70 eV, both consistent with previous measurements and calculations. We also observed a series of resonances manifest through the emission of photoelectrons with lower eKE than the direct detachment channel. The two lowest triplet states of C_6F_6 were observed and assigned to have a buckled nuclear geometry, similar to the anion ground state.

The primary features that characterised the monomer spectra were also present in those of the clusters. Specifically, the $D_0 + h\nu \rightarrow S_0 + e^-$ detachment channel was observed for n = 2 – 5 as well as the triplet states of the neutral and signatures of resonances. The increase in VDE as a function of the incremental increase in n was measured to be 200 meV

in this range, in agreement with previous studies. Resonances were also apparent in the 2D-PE spectra of clusters. The low energy PE emission seen upon the opening of the $D_0 + h\nu \rightarrow T_1/T_2 + e^-$ was argued to arise from the recapture of an outgoing photoelectron by a non-valence anion state associated with the solvent molecules.

The PE spectroscopy of $I^-(C_6F_6)$ was used to determine the rough shape of the absorption bands that appear just below the $I[^2P_{3/2}]\cdot C_6F_6 + e^-$ and $I[^2P_{1/2}]\cdot C_6F_6 + e^-$ direct detachment channels. Time-resolved PE spectra were used to probe the dynamics following excitation of the resonances just below the $I[^2P_{3/2}]\cdot C_6F_6 + e^-$ channel. This leads to the formation of a non-valence state that evolves into a valence state through a Jahn-Teller distortion along an out-of-plane buckling mode. The low energy indirect PE signal has been assigned to the excitation to an excited state of $C_6F_6^-$ at extreme buckling angles.

ACKNOWLEDGEMENTS

This work was supported by the European Research Council through Starting Grant 306536.

REFERENCES

[1] Christophorou, L. G.; Datskos, P. G.; Faidas, H. Photodetachment in the Gaseous, Liquid, and Solid States of Matter. *J. Chem. Phys.* **1994**, *101*, 6728-6742.

[2] Nyikos, L.; Ende, C. A. M.; Warman, J. M.; Hummel, A. High Mobility Excess Electrons in the Electron-Attaching Liquid Hexafluorobenzene. *J. Phys. Chem.* **1980**, *84*, 1154-1155.

[3] Gahl, C.; Ishioka, K.; Zhong, Q.; Hotzel, A.; Wolf, M. Structure and Dynamics of Excited Electronic States at the Adsorbate/Metal Interface: C_6F_6/Cu(111). *Faraday Discuss.* **2000**, *117*, 191-202.

[4] Miller, T. M.; Doren, J. M. V.; Viggiano, A. A. Electron Attachment and Detachment: C_6F_6. *Int. J. Mass Spectrom.* **2004**, *233*, 67-73.

[5] Hou, X.-J.; Huang, M.-B. Structure of the Hexafluorobenzene Anion. *J. Mol. Struct.: THEOCHEM* **2003**, *638*, 209-214.

[6] Xie, Y.; Schaefer-III, H. F.; Cotton, F. A. The Radical Anions and the Electron Affinities of Perfluorinated Benzene, Naphthalene and Anthracene. *Chem. Commun.* **2002**, *0*, 102-103.

[7] Gant, K. S.; Christophorou, L. G. Attachment of Slow Electrons to Hexa-fluorobenzene. *J. Chem. Phys.* **1976**, *65*, 2977-2981.

[8] Voora, V. K.; Jordan, K. D. Nonvalence Correlation-Bound Anion States of Spherical Fullerenes. *Nano Lett.* **2014**, *14*, 4602-4606.

[9] Rogers, J. P.; Anstöter, C. S.; Verlet, J. R. R. Ultrafast Dynamics of Low-Energy Electron Attachment via a Non-Valence Correlation-Bound State. *Nat. Chem.* **2018**, *10*, 341-346.

[10] Rogers, J. P.; Anstöter, C. S.; Verlet, J. R. R. Evidence of Electron Capture of an outgoing Photoelectron Wave by a Nonvalence State in $(C_6F_6)_n$. *J. Phys. Chem. Lett.* **2018**, *9*, 2504-2509.

[11] Dougherty, D. B.; Feng, M.; Petek, H.; Yates Jr, J. T.; Zhao, J. Band Formation in a Molecular Quantum Well via 2D Superatom Orbital Interactions. *Phys. Rev. Lett.* **2012**, *109*, 266802.

[12] Voora, V. K.; Jordan, K. D. Nonvalence Correlation-Bound Anion States of Polycyclic Aromatic Hydrocarbons. *J. Phys. Chem. Lett.* **2015**, *6*, 3994-3997.

[13] Field, D.; Jones, N. C.; Ziesel, J. P. Cold Electron Scattering in SF_6 and C_6F_6: Bound and Virtual State Channels. *Phys. Rev. A* **2004**, *69*, 052716.

[14] Suess, L.; Parthasarathy, R.; Dunning, F. B. Nondissociative Low-Energy Electron Attachment to SF_6, C_6F_6, $C_{10}F_8$, and C-C_7F_{14}: Negative Ion Lifetimes. *J. Chem. Phys.* **2002**, *117*, 11222.

[15] Eustis, S. N.; Wang, D.; Bowen, K. H.; Patwari, G. N. Photoelectron Spectroscopy of Hydrated Hexafluorobenzene Anions. *J. Chem. Phys.* **2007**, *127*, 114312.

[16] Nakajima, A.; Taguwa, T.; Hoshino, K.; Sugioka, T.; Naganuma, T.; Oho, F.; Watanabe, K.; Nakao, K.; Konishi, Y.; Kishi, R.; Kaya, K. Photoelectron Spectroscopy of $(C_6F_6)^-_n$ and $(Au\text{-}C_6F_6)^-$ Clusters. *Chem. Phys. Lett.* **1993**, *214*, 22-26.

[17] Anstöter, C. S.; Bull, J. N.; Verlet, J. R. R. Ultrafast Dynamics of Temporary Anions Probed through the Prism of Photodetachment. *Int. Rev. Phys. Chem.* **2016**, *35*, 509-538.

[18] Bull, J. N.; West, C. W.; Verlet, J. R. R. Ultrafast Dynamics of Formation and Autodetachment of a Dipole-Bound State in an Open-Shell Pi-Stacked Dimer Anion. *Chem. Sci.* **2016**, *7*, 5352-5361.

[19] Bull, J. N.; West, C. W.; Verlet, J. R. R. On the Formation of Anions: Frequency-, Angle-, and Time-Resolved Photoelectron Imaging of the Menadione Radical Anion. *Chem. Sci.* **2015**, *6*, 1578-1589.

[20] Eppink, A. T. J. B.; Parker, D. H. Velocity Map Imaging of Ions and Electrons Using Electrostatic Lenses: Application in Photoelectron and Photofragment Ion Imaging of Molecular Oxygen. *Rev. Sci. Inst.* **1997**, *68*, 3477.

[21] Even, U.; Jortner, J.; Noy, D.; Lavie, N.; Cossart-Magos, C. Cooling of Large Molecules below 1 K and He Clusters Formation. *J. Chem. Phys.* **2000**, *112*, 8068-8071.

[22] Wiley, W. C.; McLaren, I. H. Time-of-Flight Mass Spectrometer with Improved Resolution. *Rev. Sci. Inst.* **1955**, *26*, 1150-1157.

[23] Roberts, G. M.; Nixon, J. L.; Lecointre, J.; Wrede, E.; Verlet, J. R. R. Toward Real-Time Charged-Particle Image Reconstruction Using Polar Onion-Peeling. *Rev. Sci. Inst.* **2009**, *80*, 053104.

[24] Reid, K. L. Photoelectron Angular Distributions. *Annu. Rev. Phys. Chem.* **2003**, *54*, 397-424.

[25] Ervin, K. M.; Anuslewicz, I.; Skurski, P.; Simons, J.; Lineberger, W. C. The Only Stable State of O_2 Is the X $^2\Pi_g$ Ground State and It (Still!) Has an Adiabatic Electron Detachment Energy of 0.45 eV. *J. Phys. Chem. A* **2003**, *107*, 8521-8529.

[26] Gordon, S. D. S.; Osterwalder, A. 3D-Printed Beam Splitter for Polar Neutral Molecules. *Phys. Rev. Appl.* **2017**, *7*, 044022.

[27] Frisch, M. J.; Trucks, G. W.; Schlegel, H. B.; Scuseria, G. E.; Robb, M. A.; Cheeseman, J. R.; Scalmani, G.; Barone, V.; Mennucci, G. A.; Petersson, H., et al. *Gaussian 09*, Gaussian, Inc.: Wallingford, CT, 2009.

[28] Yanai, T.; Tew, D. P.; Handy, N. C. A New Hybrid Exchange-Correlation Functional Using the Coulomb-Attenuating Method (CAM-B3LYP). *Chem. Phys. Lett.* **2004**, *93*, 51-57.

[29] Dunning, T. H. Gaussian Basis Sets for Use in Correlated Molecular Calculations. I. The Atoms Boron through Neon and Hydrogen. *J. Chem. Phys.* **1989**, *90*, 1007-1023.

[30] Runge, E.; Gross, E. K. U. Density-Functional Theory for Time-Dependent Systems. *Phys. Rev. Lett.* **1984**, *52*, 997-1000.

[31] Casida, M. E. In *Recent Advances in Density Functional Methods*; Chong, D. P., Ed.; World Scientific: Singapore, 1995.

[32] Petersilka, M.; Gossmann, U. J.; Gross, E. K. U. Excitation Energies from Time-Dependent Density-Functional Theory. *Phys. Rev. Lett.* **1996**, *76*, 1212-1215.

[33] Hirata, S.; Head-Gordon, M. Time-Dependent Density Functional Theory within the Tamm-Dancoff Approximation. *Chem. Phys. Lett.* **1999**, *314*, 291-299.

[34] Hanwell, M. D.; Curtis, D. E.; Lonie, D. C.; Vandermeersch, T.; Zurek, E.; Hutchison, G. R. Avogadro: An Advanced Semantic Chemical Editor, Visualization, and Analysis Platform. *J. Cheminf.* **2012**, *4*, 17.

[35] Anstöter, C. S.; Dean, C. R.; Verlet, J. R. R. Sensitivity of Photoelectron Angular Distributions to Molecular Conformations of Anions. *J. Phys. Chem. Lett.* **2017**, *8*, 2268-2273.

[36] Wigner, E. P. On the Behavior of Cross Sections Near Thresholds. *Phys. Rev.* **1948**, *73*, 1002-1009.

[37] Anstöter, C. S.; Dean, C. R.; Verlet, J. R. R. Chromophores of Chromophores: A Bottom-up Hückel Picture of the Excited States of Photoactive Proteins. *Phys. Chem. Chem. Phys.* **2017**, *19*, 29772-29779.

[38] Stanley, L. H.; Anstöter, C. S.; Verlet, J. R. R. Resonances of the Anthracenyl Anion Probed by Frequency-Resolved Photoelectron Imaging of Collision-Induced Dissociated Anthracene Carboxylic Acid. *Chem. Sci.* **2017**, *8*, 3054-3061.

[39] West, C. W.; Bull, J. N.; Hudson, A. S.; Cobb, S. L.; Verlet, J. R. R. Excited State Dynamics of the Isolated Green Fluorescent Protein Chromophore Anion Following UV Excitation. *J. Phys. Chem. B* **2015**, *119*, 3982-3987.

[40] Nelson, D. J.; Gichuhi, W. K.; Miller, E. M.; Lehman, J. H.; Lineberger, W. C. Anion Photoelectron Spectroscopy of Deprotonated Ortho-, Meta-, and Paramethylphenol. *J. Chem. Phys.* **2017**, *146*, 074302.

[41] Gunion, R. F.; Gilles, M. K.; Polak, M. L.; Lineberger, W. C. Ultraviolet Photoelectron Spectroscopy of the Phenide, Benzyl, and Phenoxide Anions. *Int. J. Mass Spectrom. Ion Processes* **1992**, *117*, 601-620.

[42] Bochenkova, A. V.; Mooney, C. R. S.; Parkes, M. A.; Woodhouse, J. L.; Zhang, L.; Lewin, R.; Ward, J. M.; Hailes, H. C.; Andersen, L. H.; Fielding, H. H. Mechanism of Resonant Electron Emission from the Deprotonated GFP Chromophore and its Biomimetics. *Chem. Sci.* **2017**, *8*, 3154-3163.

[43] West, C. W.; Bull, J. N.; Antonkov, E.; Verlet, J. R. R. Anion Resonances Probed by photoelectron Imaging of the Para-Benzoquinone Radical Anion. *J. Phys. Chem. A* **2014**, *118*, 11346-11354.

[44] Mbaiwa, F.; Duzor, M. V.; Wei, J.; Mabbs, R. Direct and Indirect Detachment in the Iodide Pyrrole Cluster Anion: The Role of Dipole Bound and Neutral Cluster States. *J. Phys. Chem. A* **2010**, *114*, 1539-1547.

[45] Bailey, C. G.; Dessent, C. E. H.; Johnson, M. A.; Bowen, K. H. Vibronic Effects in the Photon Energy-dependent Photoelectron Spectra of the CH_3CN^- Dipole Bound Anion. *J. Chem. Phys.* **1996**, *104*, 6976-6983.

[46] Steele, D.; Whiffen, D. H. The Vibrational Frequencies of Hexafluorobenzene. *Trans. Faraday Soc.* **1959**, *55*, 369-376.

Jan Verlet was born in Leuven, Belgium. He received his MSci and PhD from King's College London in 2003 and was a post-doctoral fellow at the University of California at Berkeley. In 2006 he moved to Durham University as a lecturer and EPSRC Advanced Research Fellow and is he currently a Professor in physical chemistry. His research interests are focussed around ultrafast dynamics following photoexcitation of, photodetachment of, and electron attachment to molecules; and the development of methods to probe these dynamics in the gas-phase and at aqueous interfaces.

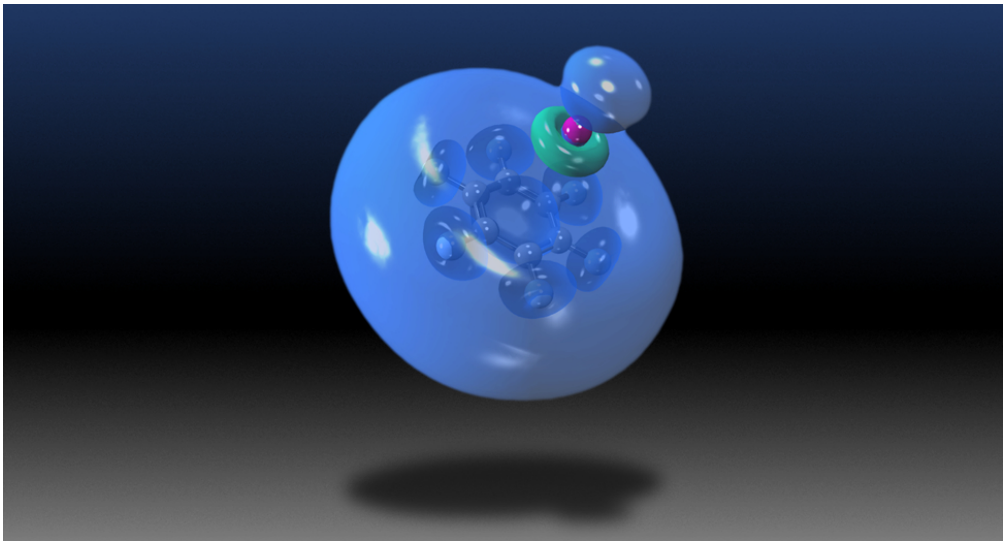

The electronic structure and dynamics of anionic hexafluorobenzene and its clusters was studied using 2D photoelectron imaging.

82x44mm (300 x 300 DPI)